



Visualization of gaseous and dissolved CO₂ migration in porous media

Jin-Seok Kim¹ · Ho Young Jo¹ · Seong-Taek Yun¹

Received: 19 September 2017 / Accepted: 7 April 2018 / Published online: 16 April 2018
© Springer-Verlag GmbH Germany, part of Springer Nature 2018

Abstract

Visualization experiments using a rectangular transparent acrylic cell, which contained glass beads saturated with alkaline solution, with a universal pH indicator, were conducted to investigate the migration behaviors of gas and dissolved CO₂ in water-saturated porous media, assuming that CO₂ exsolution occurs from the CO₂-saturated groundwater. Immediately after the CO₂ gas injection ($t < 1$ s), which is comparable to the period immediately following CO₂ exsolution, CO₂ gas moved upward, percolating into the pores through various pathways. During CO₂ gas injection ($t > 1$ s), CO₂ gas bubbles continued to move upward to the interface between the saturated porous medium and air, while dissolving in the pore water. When the CO₂ gas reached the interface, a thin, dense yellow layer was formed, followed by the gradual coalescing of the small fingers, forming a thick dense yellow layer, indicating density-driven convection. The fingers formed by the density-driven convective flow were clearer in the coarser glass beads. The migration of carbonated water was faster, as the glass bead size and the CO₂ gas injection rate increased, causing earlier CO₂ saturation in pore water. The temporal changes in the effluent CO₂ gas concentration, emitted from the saturated glass beads to air, varied with the grain size of the porous medium and the CO₂ gas injection rate.

Keywords CO₂ · Porous media · Convection · Visualization · pH indicator

Introduction

Over the past 100 years the average temperature has risen from 0.3 to 0.6 °C, with the sea level rising by 10–25 cm. If the energy use for industrial activity remains in the present condition, CO₂ emissions will gradually increase every year. One of the main causes of global warming is the greenhouse gases produced by anthropogenic activities. If the greenhouse gases continue to increase at the current level, the average temperature of earth will increase by 1.1–6.4 °C by the year 2100, with sea levels rising by 18–59 cm (IPCC 2007; IEA 2008).

Geological storage of CO₂ is a technology to sequester CO₂ in the long term by injecting captured CO₂ into large porous rock layers underground (> 800 m), with an impermeable caprock. For the geological storage of CO₂, the target porous rock layers should have a suitable depth, sufficient

porosity, and an impermeable caprock. The function of the caprock is to prevent the upward migration of the injected CO₂ by buoyancy. The injected CO₂ should be stored for long periods of time without leakage (Holoway 2005; IPCC 2007).

Even if CO₂ is sequestered in the porous rock layers with an impermeable caprock, potential risks of CO₂ leakage continue to exist. The injected CO₂ can leak through various pathways in the form of supercritical CO₂ or dissolved CO₂. CO₂ can move upward through the direct pathway around an injection well or to subsurface through the discontinuities (e.g., cracks, joints, and faults) in the caprock (Oldenburg and Lewicki 2006; Kreft et al. 2007; Gaus 2010; Plampin et al. 2014).

When CO₂ leaks through the caprocks, it dissolves into the groundwater, migrating by advection and diffusion. When the groundwater, supersaturated with CO₂, reaches the shallow subsurface, a CO₂ gas phase may be formed from the supersaturated groundwater due to a decrease in pressure, which is known as exsolution. The exsolved CO₂ gas may migrate upward through pores, fractures, and faults or re-dissolve in surrounding groundwater that is undersaturated with CO₂. The dissolution of CO₂ in groundwater can

✉ Ho Young Jo
hyjo@korea.ac.kr

¹ Department of Earth and Environmental Sciences, Korea University, 145 Anam-ro, Seongbuk-gu, Seoul 02841, Republic of Korea

significantly affect the quality of groundwater (Enouy et al. 2011; Sakaki et al. 2013; Plampin et al. 2014; Porter et al. 2015).

Previous studies have suggested two different mechanisms for gas migration in the saturated porous medium. The first was migration of gas bubbles by rising through the connected pore space induced by buoyant. The velocity of the gas migration was significantly affected by compressibility of gas (Roosevelt and Corapcioglu 1998; Corapcioglu et al. 2004; Oldenburg and Lewicki 2006; Cihan and Corapcioglu 2008). The second was migration of gas bubble trapped in the pore structure induced by the high capillary pressure of small pore throats. When the gas filled the entire pore, the pore was pressurized. The gas bubble then percolated the adjacent pore and became a gas (Li and Yortos 1995; Dominguez et al. 2000).

The evolution and migration of CO₂ gas in porous media were investigated by conducting experiments and modeling studies in the shallow subsurface (Ji et al. 1993; Brooks et al. 1999; Enouy et al. 2011; Amonette et al. 2013; Zhou et al. 2013; Sakaki et al. 2013; Plampin et al. 2014; Porter et al. 2015). For example, Ji et al. (1993) conducted the first visualization experiments using glass beads. They described gas flow pattern as a function of grain size. Brooks et al. (1999) also investigated gas flow pattern using glass beads ranged between 0.42 and 3 mm. They showed coherent gas flow occurred for small grain size, whereas incoherent gas flow occurred for large grain size. Sakaki et al. (2013) conducted experiments using 4.5-m-long columns filled with different sizes of sands. CO₂-saturated water was injected into the bottom of the columns, while monitoring the water saturation, electrical conductivity (EC), and temperature. They indirectly showed the formation of gas phase in the columns, regardless of the size of sands, by providing water saturation data. The gas formation was affected by the CO₂ saturation pressure in the injected water and the hydrostatic pressure. The gas formation was enhanced when the CO₂ saturation pressure was higher than the hydrostatic pressure.

Most studies regarding CO₂ migration in the reservoir focused on the characterization and visualization of density-driven, subsurface CO₂ migration due to buoyancy (Kneafsey and Pruess 2009; Polak et al. 2011; Bang et al. 2012; Faisal et al. 2013; Mojtaba et al. 2014; Thomas et al. 2015). The main purpose of the studies was to characterize convective CO₂ migration in subsurface areas, where supercritical or gaseous CO₂ was dissolved in saline water. However, few studies have showed visually, the behaviors of the leaked CO₂ gas (i.e., CO₂ gas migration and re-dissolution) in shallow aquifers, consisting of porous media (Bang et al. 2012). Bang et al. (2012) investigated the visually leaked CO₂ migration in porous media using a thin, transparent tank, filled with water-saturated glass beads, containing a universal pH indicator, which changed color with the change in pH

of water. The CO₂ gas was injected through a needle in the bottom of the tank. The gas and the dissolved CO₂ migration patterns were monitored using digital cameras during testing. They visually showed the patterns of CO₂ gas migration and the convection of carbonated water in the glass beads, which were affected by the size of the glass beads.

The objectives of this study were to observe directly the patterns of CO₂ gas migration, re-dissolution, and dissolved CO₂ migration in the water-saturated porous medium, while investigating the effects of the size of the porous medium and CO₂ injection rate on the migration patterns and effluent CO₂ gas concentration from the porous medium. This study assumed that the CO₂ leaked from the reservoir reaches the shallow aquifer, causing CO₂ gas formation due to a decrease in pressure.

Materials and methods

Materials

Two sizes of finer and coarser glass beads (DAIHAN Scientific) were used to investigate the effect of pore size on the gaseous and dissolved CO₂ migration in the porous medium. Sieve analyses, conducted on the glass beads using ASTM D 422-63 (2007), show that the sizes of finer and coarser glass beads ranged from 0.25 to 0.5 mm and from 0.75 to 1.0 mm, as shown in Fig. 1a. The soil–water characteristic curves (SWCC) for the glass beads were determined using a hanging column test, followed by ASTM D 6836-16 (2016) as shown in Fig. 1b. The SWCC describes the relationship between volumetric water content and suction. The finer glass beads had a higher air entry suction than the coarser glass beads due to their smaller pore size, indicating that the finer glass beads (1.4 kPa) had a higher capillary pressure than coarser glass beads (0.6 kPa).

The physical properties of glass beads are shown in Table 1. The porosities of finer and coarser glass beads were 0.40 and 0.38, respectively, with packing densities of 1.50 and 1.59 g/cm³, respectively. The hydraulic conductivities of finer and coarser glass beads were 1.7×10^{-2} and 5.8×10^{-2} cm/s, respectively, which were measured by the constant head method.

De-ionized (DI) water (pH = 5.6) was used to saturate the glass beads. Concentrated NaOH solution was added to the DI water for adjusting the pH to approximately 10. A universal pH indicator was used to visualize the change in pH due to CO₂ dissolution and the migration of carbonated water in porous media. The universal pH indicator is a mixture of several chemical compounds that cause smooth color changes to occur as the pH of the solution changes from 1 to 14. A universal pH indicator is typically composed of water, propan-1-ol, phenolphthalein sodium salt, sodium

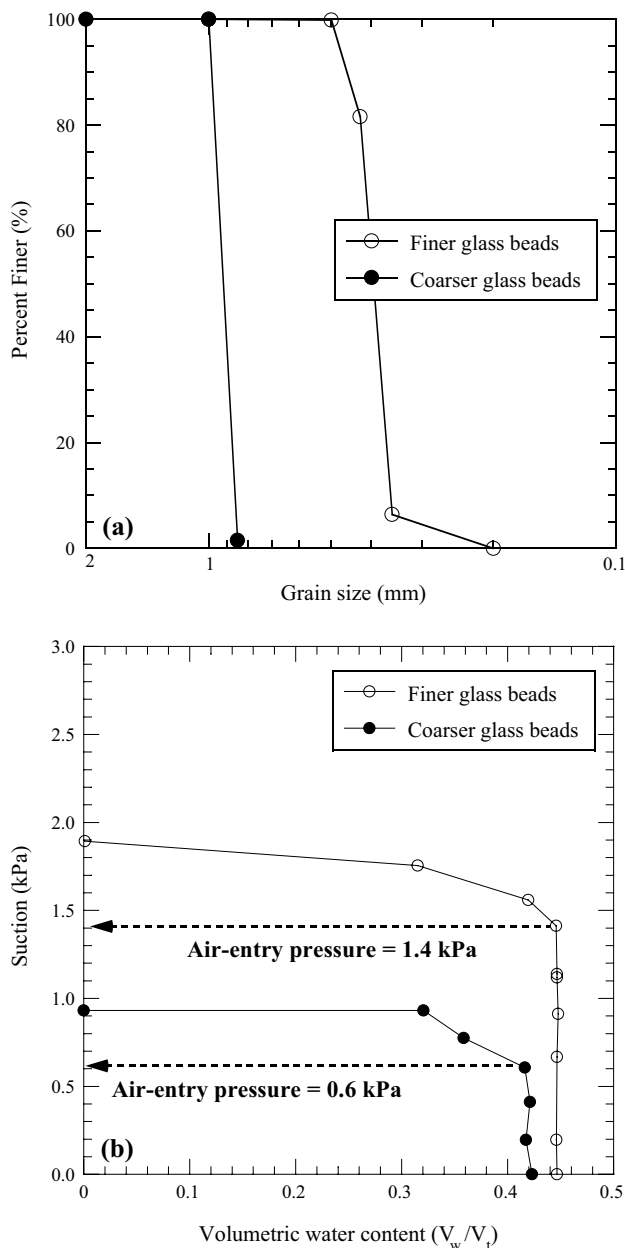


Fig. 1 Grain size distribution curves (a) and soil–water characteristics curves (SWCC), (b) for finer and coarser glass beads

Table 1 Physical properties of glass beads used in this study

Glass bead size (mm)	Physical properties		
	Porosity	Packing density (g/cm ³)	Hydraulic conductivity (cm/s)
0.25–0.5 (finer)	0.40	1.50	1.7×10^{-2}
0.75–1.0 (coarser)	0.38	1.59	5.8×10^{-2}

hydroxide, methyl red, bromothymol blue monosodium salt, and thymol blue monosodium salt. Yellow to red, red to green, and green to blue or purple indicate that the solution is acidic, neutral, and alkaline, respectively (Foster and Grunfest 1937).

Visualization experiments for CO₂ gas and dissolved CO₂ migration

A series of visualization experiments were conducted to investigate the effect of the grain size of porous medium and the CO₂ gas leakage rate on the gaseous and dissolved CO₂ migration in the water-saturated porous medium. A schematic diagram of the experiment is shown in Fig. 2. A rectangular transparent acrylic cell (width × height × thickness = 25 cm × 25 cm × 5 cm) was filled with glass beads, up to a height of 20 cm in the cell to allow constant head space. The head space (25 cm × 5 cm × 5 cm) was filled with air. The glass beads in the cell were subsequently saturated with a mixture of an alkaline solution (pH = 10) and a universal pH indicator. After adding the universal pH indicator to the alkaline solution, the color of the solution turned purple, indicating a pH of 10. The alkaline solution for saturating the glass beads was used to clearly observe the migration of dissolved CO₂ because the dissolution of CO₂ in the solution caused changes to the pH.

Approximately 99.99% purity of CO₂ gas was injected at 3 cm from the bottom of the cell to simulate CO₂ gas exsolution in shallow aquifer, using Teflon tubing, which has low CO₂ sorption capacity. CO₂ was injected at various injection rates (20, 40, 100, and 200 cm³/min) to evaluate the effect of gas leakage rate on the CO₂ gas and dissolved CO₂ migration in the porous medium. When supercritical CO₂ or CO₂-saturated groundwater leaks through discontinuities in the confined layer, the CO₂ gas leakage rate can vary, depending on the pressure decrease rate (Sakaki et al. 2013). The CO₂ injection rate was controlled by a gas mass controller (Alicat Scientific, Inc.). The CO₂ gas and dissolved CO₂ migration were filmed using a digital camera (Cam Shots) during the experiment. The empty headspace of the captured images was removed to show more closely the phenomena occurred in the porous media.

The reactor had a sealing cap at the top to prevent CO₂ gas leakage. However, the sealing cap had a small hole, which was connected to an infrared (IR)-based CO₂ analyzer (LI-820 IR CO₂ analyzer), to measure effluent CO₂ gas concentration emitted from the saturated glass beads. The effluent CO₂ gas concentration was logged automatically by a computer at every second. The effluent CO₂ gas was diluted 10 times using 99.9% purity of N₂ gas for lowering the effluent CO₂ gas concentration, to satisfy the maximum CO₂ detection limit of the analyzer. The effluent CO₂ gas

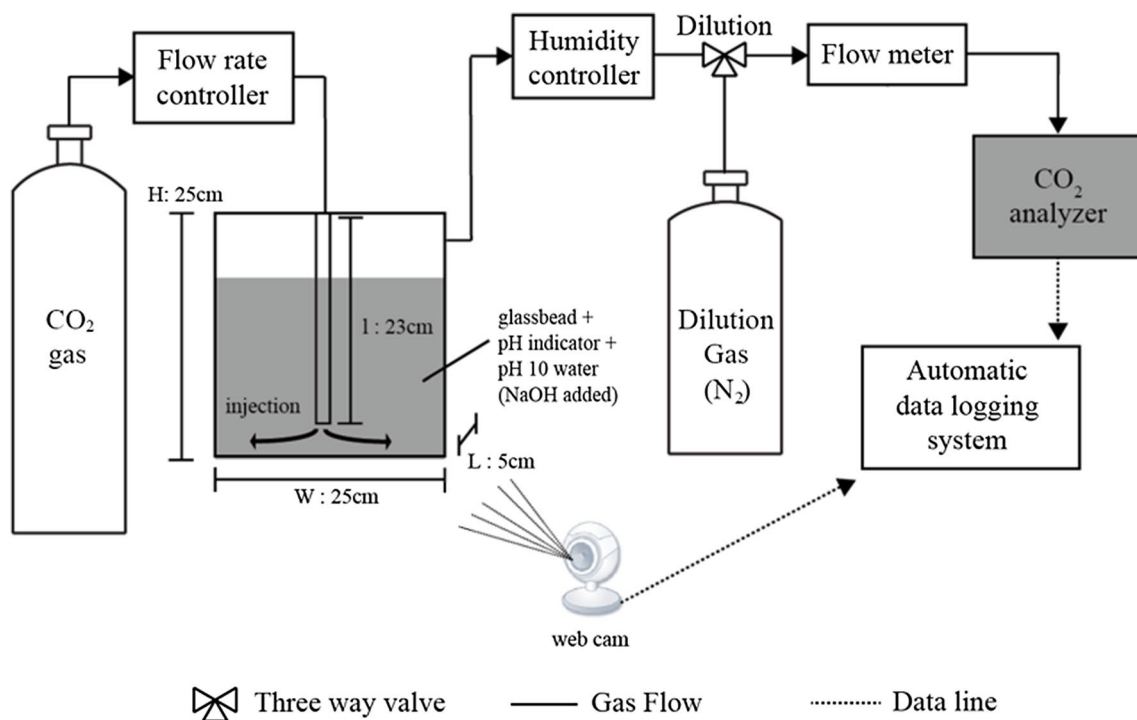


Fig. 2 Schematic diagram of a visualization experiment setup

was dehydrated by using a column containing silica gel to minimize errors in the measurement (Fig. 2).

Results and discussion

Visualization of CO₂ gas and dissolved CO₂ migration

At the beginning of the CO₂ gas injection: CO₂ gas movement

At the beginning of the CO₂ gas injection ($t < 1$ s), the movement of gas bubbles through the glass beads was observed, regardless of the grain size and CO₂ injection rate (20–200 cm³/min). However, no color change was observed in the pore water, indicating that the CO₂ dissolution did not occur immediately after CO₂ gas injection (Fig. 3). For the coarse glass beads (0.75–1 mm), as the CO₂ injection rate increased, the plume of CO₂ gas bubbles was more clearly observed, with the lateral extent of the plume becoming larger (Fig. 3). On the other hand, the movement of gas bubbles could not be observed clearly for the finer glass beads, when the CO₂ gas injection rate was low (20–40 cm³/min). The movement of gas bubbles can be initiated when the injection pressure is higher than the air entry pressure (i.e.,

hydrostatic and capillary pressures) induced by the saturated porous beads (Geistlinger et al. 2006).

When CO₂ gas was injected into the glass beads at a higher injection pressure than the air entry pressure, CO₂ gas moved upward due to buoyancy and pressure gradient, percolating into various pathways. CO₂ gas displaced the water in the pores of the glass beads, producing irregular continuous gas pathways, like trees. The tree-like pattern induced by air injection to saturated medium is called “channelized flow,” in which the air displaces water along continuous pathways of least resistance. Various factors, such as grain size, packing density, and injection rate, can affect the channelized flow pattern (Ji et al. 1993; Brooks et al. 1999). Brooks et al (1999) suggested that the channelized flow occurred when the grain size and injection rate were less than 1.5 mm and higher than 10 cm³/min, respectively. In this study, the channelized flow pattern was more clearly observed in the glass beads with larger grain size (0.75–1.0 mm).

During the CO₂ gas injection: CO₂ gas and dissolved CO₂ migration

The representative images of temporal changes in the CO₂ gas and dissolved CO₂ (i.e., carbonated water) migration for the finer glass beads (0.25–0.5 mm) at various CO₂ gas injection rates from 20 to 200 cm³/min are shown in Fig. 4. Immediately after CO₂ gas injection ($t > 1$ s), CO₂ gas

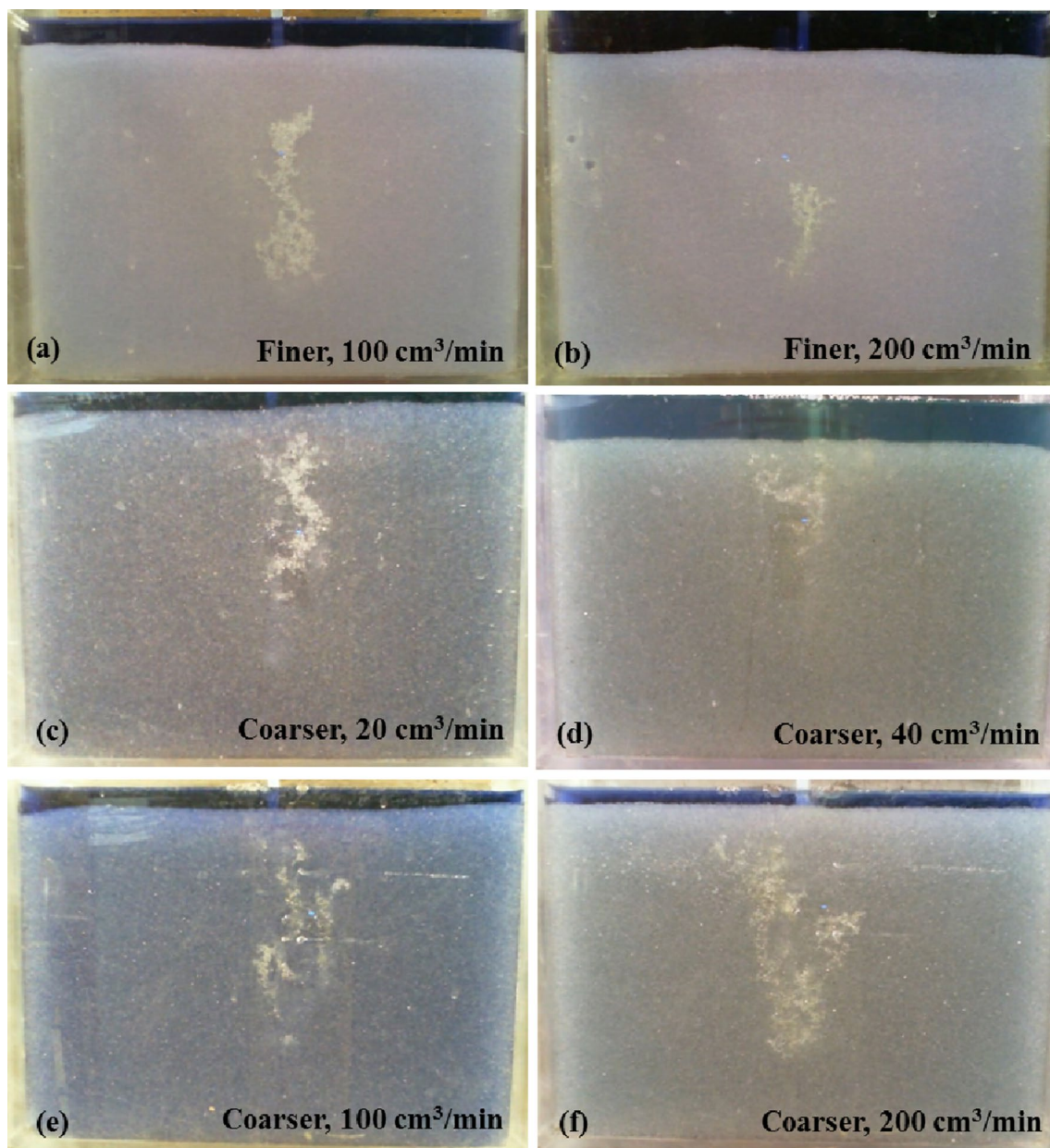


Fig. 3 Captured images of CO₂ gas migration in finer (0.25–0.5 mm, **a, b**) and coarser (0.75–1 mm, **c–f**) glass beads, from the visualization experiments at various CO₂ injection rates at the beginning of CO₂ injection ($t < 1$ s)

bubbles continued to move upward to the top surface, with the color of pore water near the pathways of CO₂ gas bubbles changing from blue to yellow, regardless of the injection rate, suggesting that CO₂ dissolution began in pore water near the CO₂ gas migration pathways.

Figure 5 shows the enlarged images of areas near the surface of the cell during CO₂ injection for the finer glass beads (0.25–0.5 mm). CO₂ bubble movement in the glass beads was continuously observed during the CO₂ gas injection. CO₂ bubbles coalesced to form clusters, moving through the glass beads as clusters. Once the clusters reached the

top surface of the glass beads (i.e., the interface between water-saturated glass beads and air), the glass beads on the top surface explode due to the expulsion of CO₂ gas by displacing water. At the lowest CO₂ gas injection rate of 20 cm³/min, weak explosion was observed, probably because the amount of injected CO₂ was not sufficient to form gas clusters, causing the continuous channelized CO₂ gas flow or/and the injection pressure to be lower than the overburden pressure (Fig. 5). On the other hand, at a high injection rate, ranging between 40 and 200 cm³/min, larger CO₂ clusters were formed, causing the glass beads on the

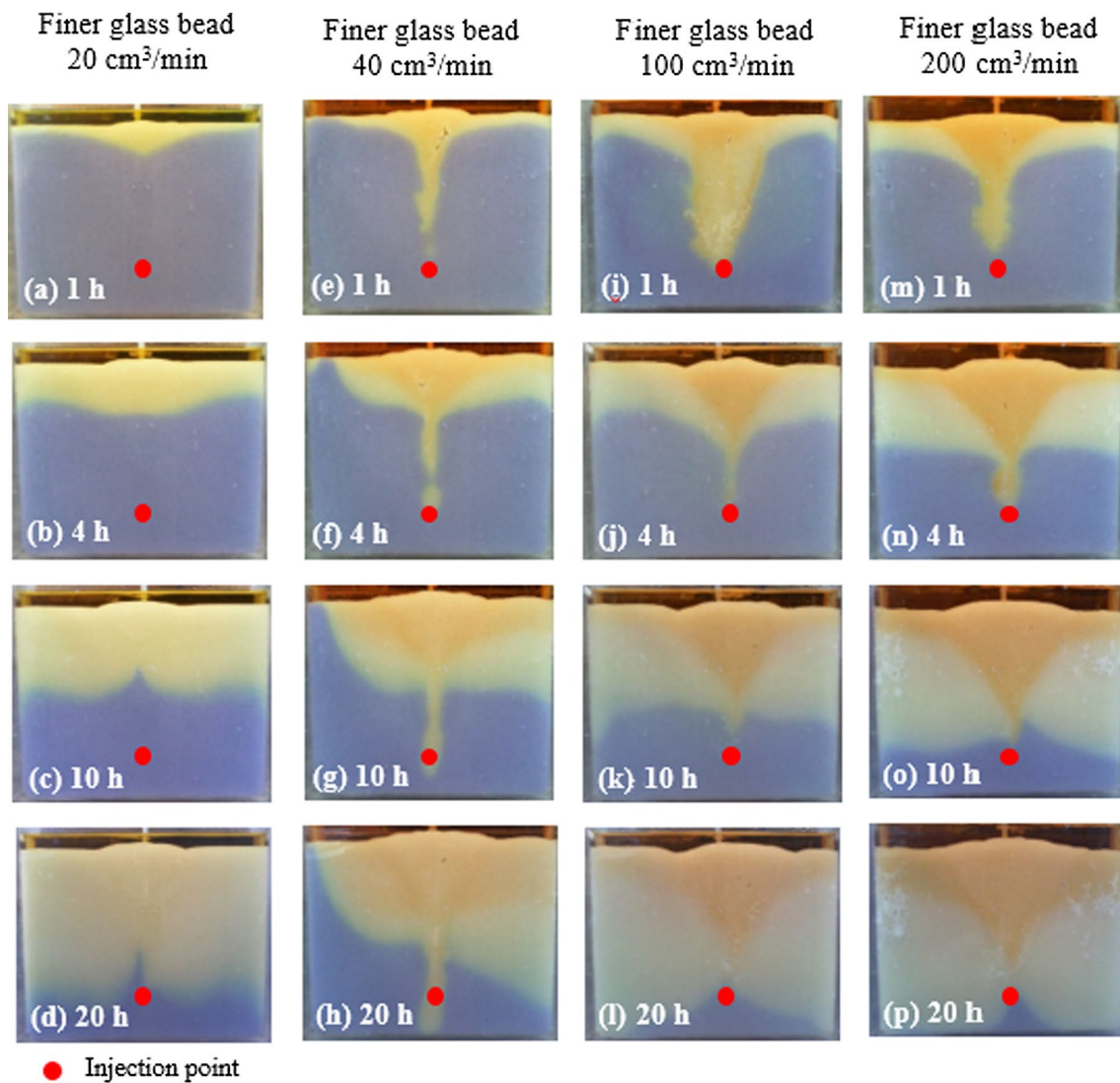


Fig. 4 Captured images from the visualization experiments using finer glass beads (0.25–0.5 mm) at various CO₂ injection rates during CO₂ injection ($t > 1$ s)

surface to swell, subsequently explosion. The expansion and explosion of clusters occurred rapidly as the CO₂ gas injection rate increased (Fig. 4). The top surface of the glass beads explodes because the upward pressure of CO₂ bubbles exceeded the overburden pressure due to buoyancy and advection.

The color of the pore water changed from blue to yellow, indicating CO₂ dissolution during CO₂ injection (Fig. 5), regardless of the CO₂ injection rate. The color of pore water in the glass beads changed with the pH of the pore water because the pore water contained the universal pH indicator (Fig. 5). The initial pH of the pore water in the glass beads was 10, causing the color of the pore water to be blue. When CO₂ was injected into the glass beads, the color of the pore water turned from blue to yellow, as the pore water changed from alkaline to acidic. The color change suggests that CO₂

dissolution occurred in the pore water, causing a decrease in the pH of the pore water, while producing carbonated water. The darker yellow of the pore water indicates that more CO₂ dissolved in the pore water.

For the CO₂ injection rate of 20 cm³/min, at time = 1 h, carbonated water (yellow) was produced on the top surface by CO₂ dissolution, laterally extending by advection and diffusion, forming a thin, dense layer on the interface between the saturated glass beads and air. The yellow layer was darker near the injection tube, indicating more CO₂ dissolution. After the formation of the thin, dense yellow layer, small fingers were formed, suggesting the initiation of density-driven convection. The small fingers then gradually coalesced, forming a thick, dense yellow layer (Fig. 4).

As the CO₂ injection rate increased from 40 to 200 cm³/min, the color change occurred more clearly near the

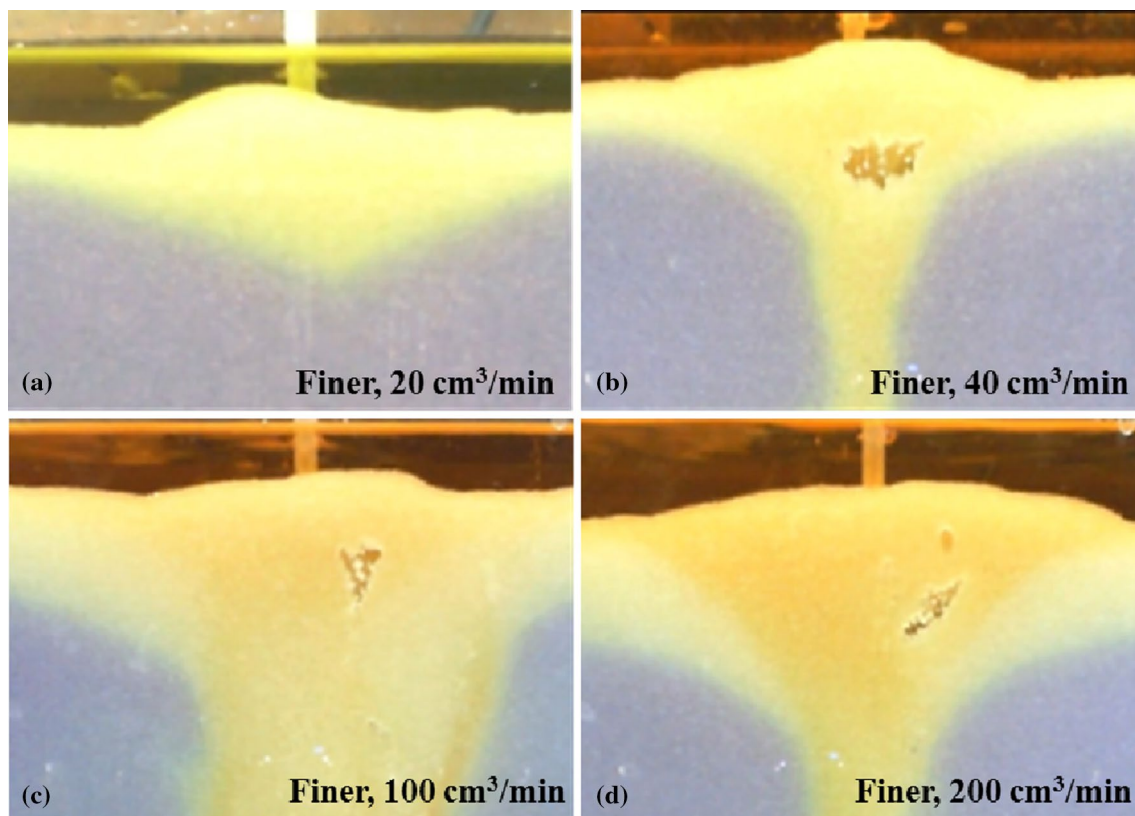


Fig. 5 Enlarged images showing CO₂ gas clusters obtained from the visualization experiments using finer glass beads (0.25–0.5 mm) at various CO₂ injection rates during CO₂ injection ($t \geq 1$ h)

injection tube, suggesting that CO₂ dissolution occurred near the channelized CO₂ gas flow pathways (i.e., plume of CO₂ gas and dissolved CO₂; Fig. 4). The plume extent of the dissolved CO₂, which had an inverted triangle shape, increased with the increase in CO₂ gas injection rate. The dense layer formed near the interface thickened with time due to the density-driven convection of carbonated water. The downward migration of carbonated water was faster with the increase in CO₂ gas injection rate. The downward migration along the side wall was probably faster because the pore size along the side wall was larger than that inside the glass beads.

For coarse glass beads (0.75–1.0 mm), no large bubble clusters were observed. However, more continuous channelized CO₂ gas flow pathways were observed during CO₂ gas injection (Fig. 6), potentially because the air entry pressure of the coarser glass beads was smaller than that of the finer glass beads as shown in Fig. 1b. Similar to the finer glass beads (0.25–0.5 mm), the CO₂ gas moved upward to the top surface by buoyancy and advection, while CO₂ dissolution began near the CO₂ gas bubble migration pathways. The carbonated water produced by CO₂ dissolution on the interface between the glass beads

and air was laterally extended due to advection and diffusion, forming a single dense layer on the top surface.

The downward migration of the carbonated water due to the density-driven convective flow was divided into three patterns during CO₂ injection for the coarser glass beads, probably due to their higher hydraulic conductivity: (1) downward migration along the side wall, (2) downward migration of the dense layer, and (3) direct downward migration from the CO₂ injection point to the bottom of the cell, causing a triangular-shaped accumulation. The triangular-shaped accumulation was not clearly observed in the experiment with the high CO₂ injection rate of 200 cm³/min. The boundary layer at the interface between carbonated water and pre-existing water became unstable, producing small fingers, which were induced by density-driven convective flow. The denser fingers produced a plume by coalescing small fingers, with the plume moving downward. During the downward movement of the plume, lateral concentration difference occurred with the plumes descending into the surrounding water. Therefore, the density of the descending plumes was reduced, along with the concentration flux, relative to the initial level (Neufeld et al. 2010). The formation of fingers by the density-driven convective flow was more clearly observed in the coarser glass

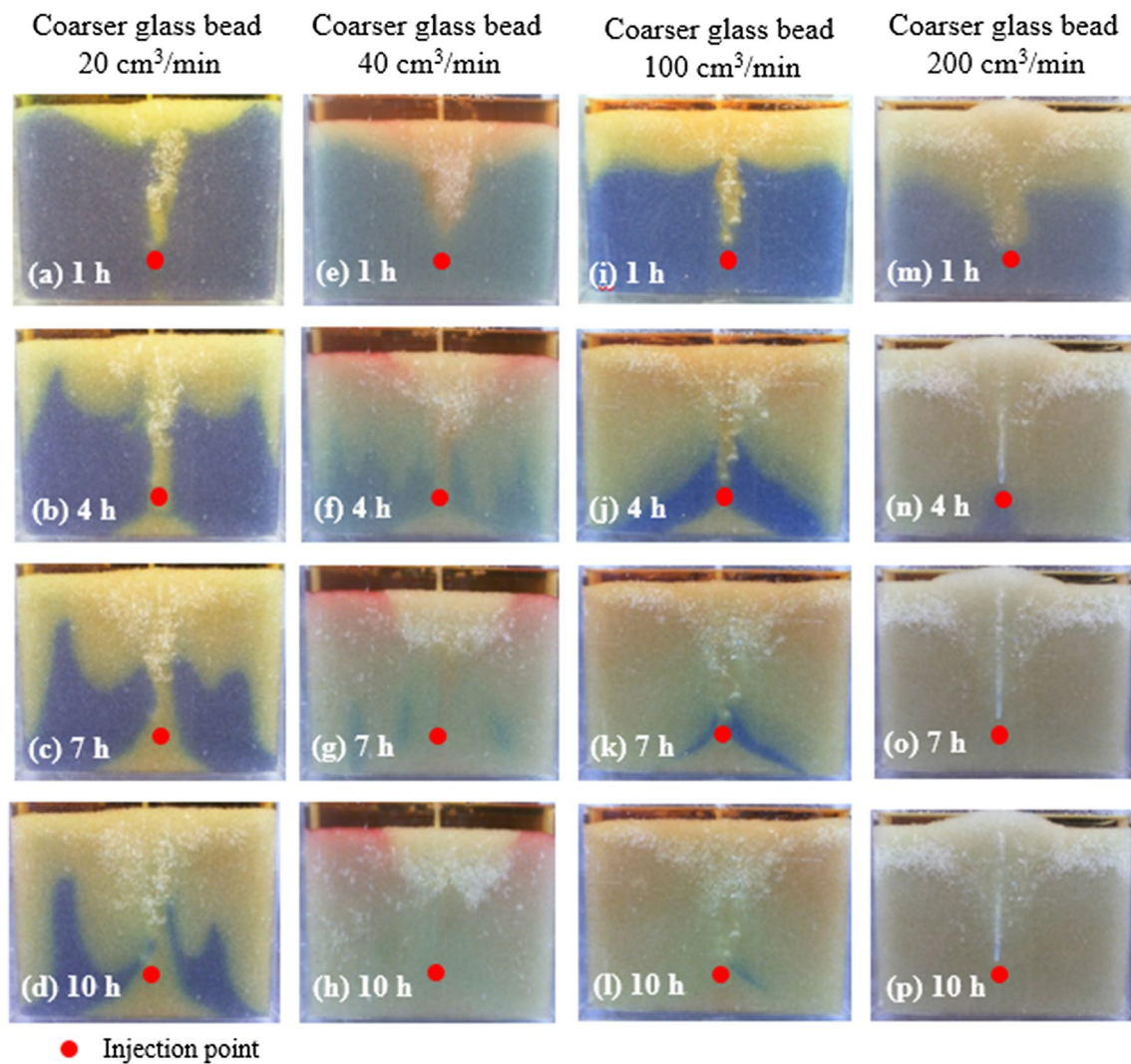


Fig. 6 Captured images from the visualization experiments using coarser glass beads (0.75–1.0 mm) at various CO₂ injection rates during CO₂ injection ($t > 1$ s)

beads, suggesting that the density-driven convective flow was more dominant in them. Finally, the glass beads were fully saturated with carbonated water. The migration of carbonated water was faster as both, the glass bead size and the CO₂ gas injection rate, increased, causing earlier CO₂ saturation in the pore water.

Packing stability

The growth of the plume of CO₂ gas and dissolved CO₂ near the injection tube (i.e., fluidized zone or inverted triangular-shaped zone) and the explosion on the top surface of the glass beads can be quantitatively evaluated using the packing stability of the unconsolidated porous medium, which can be

calculated using the packing stability ratio of V_d to V_c , determined by the following equations (Zhao 2010).

$$V_d = \frac{Q}{\pi a(H_b - H_{or})} \quad (1)$$

$$V_c = \frac{(\rho_{gb} - \rho_w)(1 - \Phi)}{\rho_w} k_w \quad (2)$$

where Q is the air injection rate, a is the thickness of the saturated glass beads, $H_b - H_{or}$ is the effective height of the saturated porous glass beads. ϕ is the porosity of the saturated porous medium, ρ_{gb} is the packing density of the glass beads, ρ_w is the density of water, and k_w is the initial

Table 2 Calculated packing stability ratios for the glass beads at various CO₂ injection rates

Glass bead size (mm)	Packing stability ratio (V_d/V_c)			
	20 cm ³ /min	40 cm ³ /min	100 cm ³ /min	200 cm ³ /min
0.25–0.5 (finer)	0.23	0.47	1.17	2.34
0.75–1.0 (coarser)	0.06	0.12	0.30	0.60

hydraulic conductivity of the glass beads. V_d is the dipole velocity related to air flow, and V_c is the critical velocity related to uplift of a patch of grains. If V_c is less than V_d , the grain patch can be uplifted. Because the air flow can cause instability of the matrix, the grain patch can be uplifted and pushed by the air flow. The calculated packing stability ratio, V_d/V_c , is shown in Table 2. An increase in the packing stability ratio suggests that the stability of the saturated glass beads for a given test condition (i.e., glass bead size and CO₂ gas injection rate) decreases during CO₂ gas injection.

The packing stability ratio increased, suggesting that the stability of the saturated glass beads decreased due to the CO₂ gas injection, as both, the glass bead size and the CO₂ gas injection rate, increased (Table 2). As the packing stability increased, the inverted triangular-shaped zone (i.e., plume of CO₂ gas and dissolved CO₂) at the top of glass beads appeared more clearly (Figs. 4 and 6). For the finer glass beads (0.25–0.5 mm), the inverted triangular-shaped zone appeared clearly when the packing stability ratio was higher than approximately 0.5, at a CO₂ gas injection rate higher than 40 cm³/min. Above the injection point, an unstable packing zone was formed with the increase in packing instability, leading to an inverted triangular-shaped zone at the top surface of the glass beads.

For example, for the finer glass beads (0.75–1 mm) at CO₂ gas injection rates of 100 and 200 cm³/min, the packing stability ratio was higher than 1, suggesting that the packing instability was too large to hold the grains in the initial position. As a result, a fluidized zone was formed in the glass beads near the injection tube, above the CO₂ injection point, with dissolution occurring more actively in the fluidized zone (Fig. 4). The formation of the fluidized zone during CO₂ gas injection could be clearly observed by the change in color induced by CO₂ dissolution. In addition, the explosion at the top surface of the glass beads clearly occurred when the packing ratio was higher than 0.5. For the finer glass beads, this occurred at a CO₂ gas injection rate higher than 40 cm³/min, while for the coarser glass beads, it occurred at a CO₂ injection rate of 200 cm³/min (Figs. 4 and 6), suggesting that the packing instability caused the explosion.

Effluent CO₂ concentrations

The temporal changes in the normalized effluent CO₂ gas concentration, obtained from the experiments using the finer

and coarser glass beads, are shown in Figs. 7 and 8. The normalized effluent CO₂ gas concentration was the ratio of the effluent CO₂ gas concentration ($[\text{CO}_2]_e$) to the initially injected CO₂ gas concentration ($[\text{CO}_2]_i$).

The gas flow patterns, through a saturated porous medium, are classified as transient and steady drainage phases. When CO₂ is injected into a saturated porous medium, CO₂ displaces water, becoming trapped in the pore spaces. When the CO₂ gas pressure exceeds the overburden pressure, CO₂ moves upward along the preferential pathways of least resistance. When the CO₂ gas is emitted from the saturated porous medium, with the effluent CO₂ gas concentration exceeding the influent CO₂ gas concentration, it is called the transient drainage phase. After the transient drainage phase, the CO₂ gas flow enters a steady-state phase (Geistlinger et al. 2006).

For the finer glass beads (0.25–0.5 mm), at a CO₂ gas injection rate of 20 cm³/min, the breakthrough of CO₂ gas concentration occurred at an early stage of the experiment (2–6 h), with a significant drop in the effluent CO₂ concentration subsequently (Fig. 7a). The early initial breakthrough could probably be attributed to the continuous channelized CO₂ gas flow, resulting in the CO₂ gas reaching the top surface early. CO₂ gas bubbles on the top surface of the glass beads at 20 cm³/min are shown in Fig. 4a–d. Subsequently, a significant drop in the effluent CO₂ concentration occurred due to gradual CO₂ dissolution in the pore water of the glass beads, retarding the CO₂ gas emission. At the CO₂ gas injection rates of 40 and 100 cm³/min, lower normalized effluent CO₂ gas concentration occurred at an early stage, compared to that at 20 cm³/min, eventually stabilizing (Fig. 7a–c), probably because the CO₂ gas bubbles coalesced, forming clusters and retarding the gas bubble migration, causing the CO₂ gas to dissolve in the pore water. CO₂ gas clusters were observed in the experiments at 40 and 100 cm³/min. However, they were not observed at 20 cm³/min, as shown in Fig. 5. On the other hand, at a CO₂ gas injection rate of 200 cm³/min, early breakthrough occurred within 1 h, with no subsequent change in the effluent CO₂ gas concentration (Fig. 7d), which suggests that CO₂ gas continuously migrated upward, emitting from the glass beads due to the higher CO₂ gas injection rate. While CO₂ gas bubbles were observed, no cluster was observed in the CO₂ gas pathways in the experiment at 200 cm³/min, as shown in Fig. 5.

For the coarser glass beads (0.75–1.0 mm), earlier and more CO₂ gas emission occurred from the saturated glass

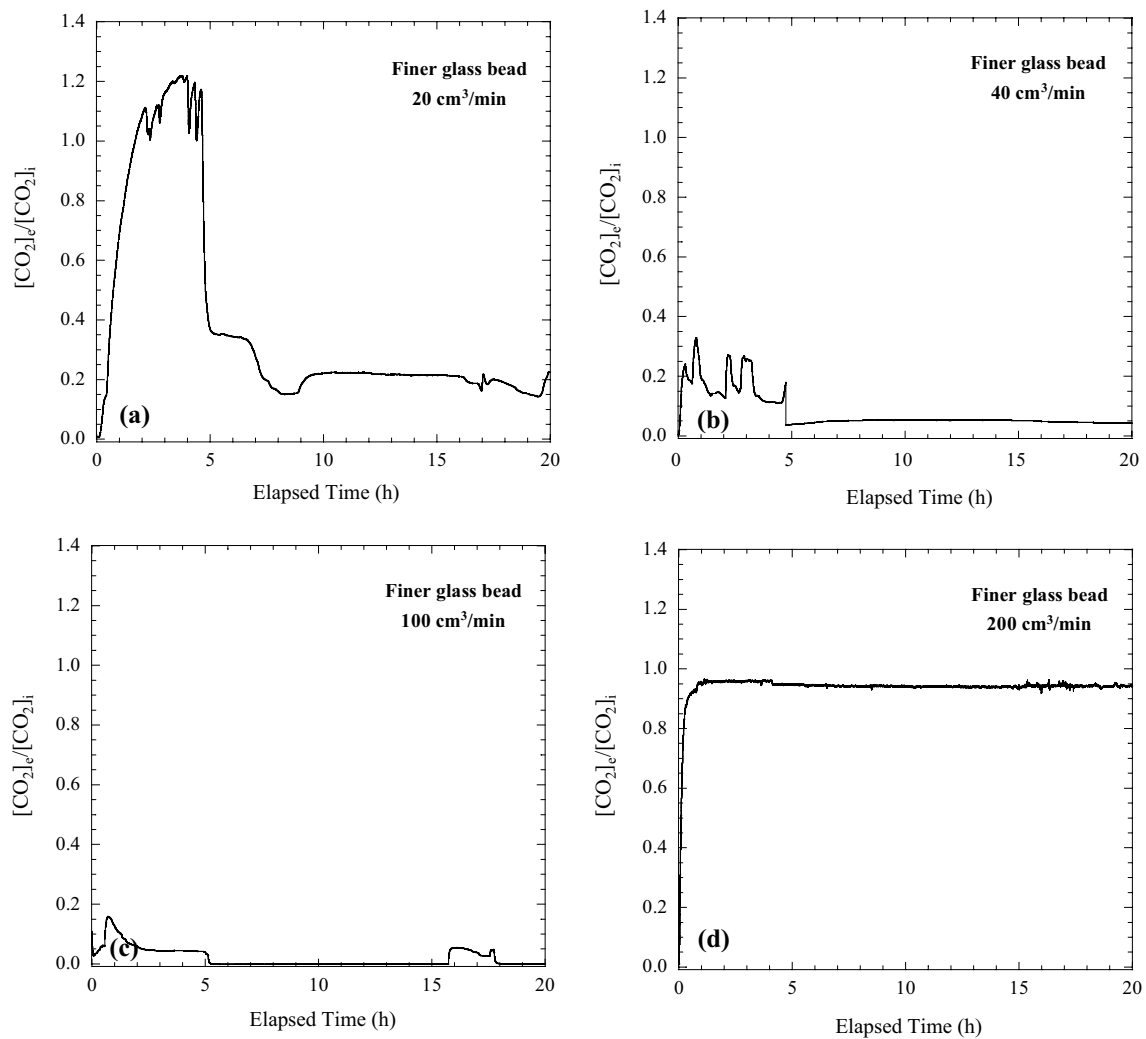


Fig. 7 Ratio of the effluent CO₂ concentration ($[\text{CO}_2]_e$) to influent CO₂ concentration ($[\text{CO}_2]_i$) as a function of the time elapsed, obtained from the visualization experiments using finer glass beads (0.25–0.5 mm) at various CO₂ injection rates

beads than the finer glass beads (0.25–0.5 mm) at a given CO₂ gas injection rate, except for 20 cm³/min (Fig. 8). At a CO₂ injection rate of 20 cm³/min, almost no CO₂ gas was emitted from the saturated glass beads during the CO₂ gas injection (Fig. 8a), suggesting that the injected CO₂ gas was trapped in the pore space, dissolving in the pore water. After approximately 9 h, when the pore water was almost saturated with CO₂, a very small amount of CO₂ was emitted (Figs. 6 and 8). In the larger glass beads, the fluidized zone (plume of CO₂ gas and dissolved CO₂) was further extended due to the larger pore space, leading to lower CO₂ gas emission. At 40 cm³/min, a fluctuation was observed in the effluent CO₂ gas concentration during CO₂ injection, indicating transient CO₂ gas flow (Fig. 8b). CO₂ gas was trapped in the pore, subsequently dissolving in the pore water near CO₂ gas migration pathways. When the buoyant pressure exceeded the air entry and overburden pressures, CO₂ gas was emitted

from the saturated glass beads, leading to an increase in the effluent CO₂ concentration. These transient CO₂ flow processes were repeated, causing a fluctuation in the effluent CO₂ gas concentration. At the CO₂ injection rate of 200 cm³/min, almost no transient CO₂ flow was observed. However, a steady-state CO₂ flow was achieved rapidly (Fig. 8d).

The cumulative mass of dissolved CO₂ with time at different CO₂ injection rates was calculated using the effluent CO₂ gas concentration ($[\text{CO}_2]_e$) and the initially injected CO₂ gas concentration ($[\text{CO}_2]_i$). The cumulative mass of dissolved CO₂ with time is shown in Fig. 9. The highest and lowest cumulative masses of dissolved CO₂ were obtained at the CO₂ injection rates of 100 and 20 cm³/min, respectively, regardless of the glass bead size. The cumulative mass of dissolved CO₂ increased with increasing the CO₂ injection rate. However, the cumulative mass of dissolved CO₂ at 200 cm³/min was lower than those at 40 and 100 cm³/

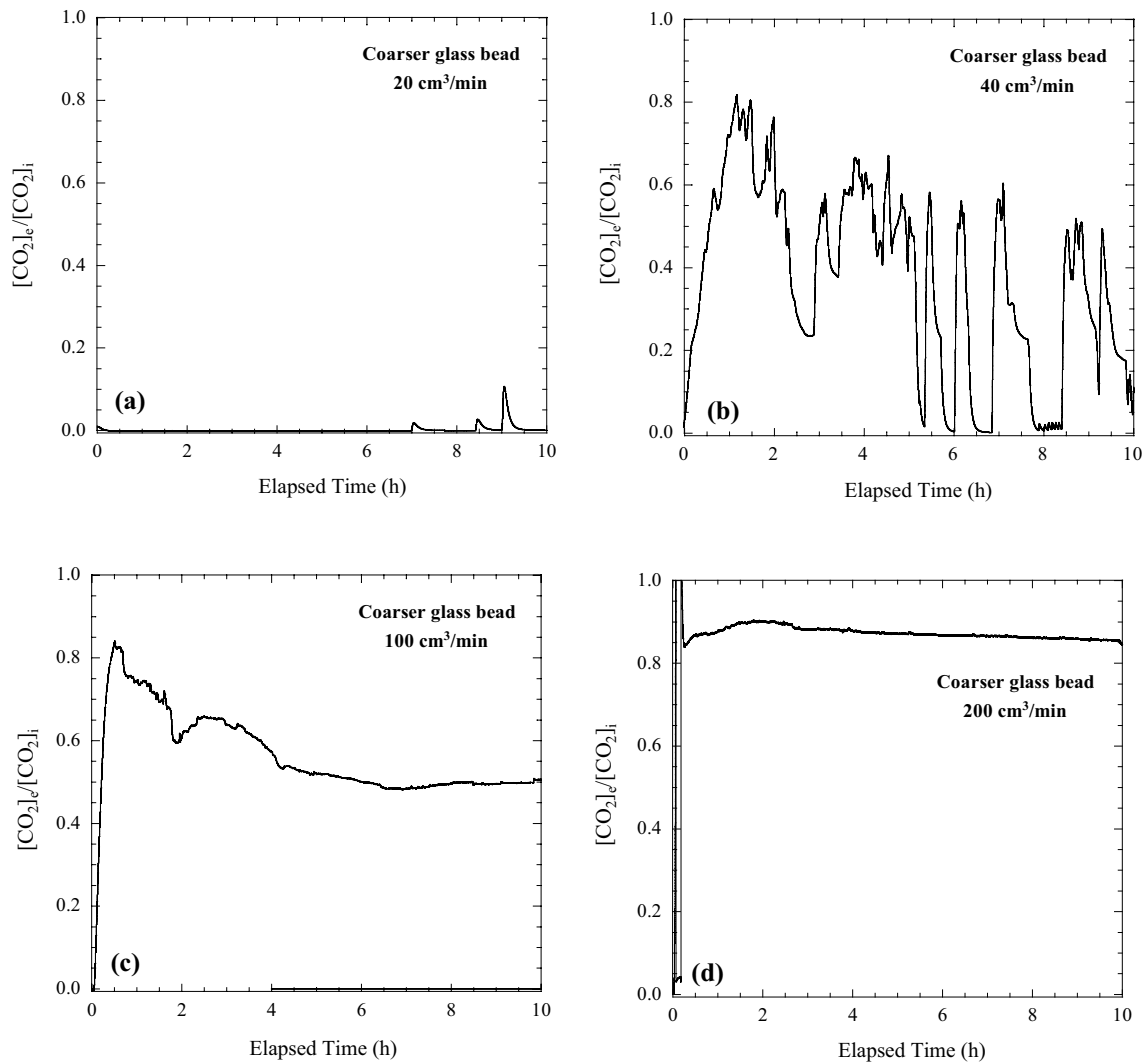


Fig. 8 Ratio of the effluent CO_2 concentration ($[\text{CO}_2]_e$) to influent CO_2 concentration ($[\text{CO}_2]_i$) as a function of the elapsed time, obtained from the visualization experiments using coarser glass beads (0.5–1.0 mm) at various CO_2 injection rates

min. The results of the cumulative mass of dissolved CO_2 were comparable to those of the normalized effluent CO_2 gas concentration (Figs. 7, 8, 9). At the low CO_2 injection rate, the incoherent flow occurs due to buoyancy, causing lower CO_2 dissolution. As the CO_2 injection rate increases, the incoherent flow becomes gradually the coherent flow, causing an increase in the CO_2 dissolution. However, when the CO_2 injection rate exceeds the critical CO_2 injection rate, the multiple channels coalesce into single channel (Geistlinger et al. 2006), probably causing a decrease in the CO_2 dissolution.

Implication

The injected CO_2 can leak through caprock, subsequently dissolving in the surrounding groundwater, producing

CO_2 -saturated groundwater. The CO_2 -saturated groundwater can move upward through discontinuities such as fractures and faults, which can produce significant changes in pressure. A significant pressure drop causes the exsolution of CO_2 gas from the CO_2 -saturated groundwater. The CO_2 exsolution rate from the leaking point can vary with the pressure drop in the CO_2 -saturated groundwater. Higher pressure drop can lead to a higher CO_2 exsolution rate. In this study, the CO_2 exsolution rate was simulated with the CO_2 injection rate.

The exsolved CO_2 gas moves upward due to buoyancy and pressure gradient in the shallow aquifer containing the porous media. After the early stage of CO_2 gas leak from the exsolution point, the CO_2 gas bubbles initially percolate into the porous media through various pathways, subsequently leading to CO_2 dissolution near the CO_2 gas pathways. The

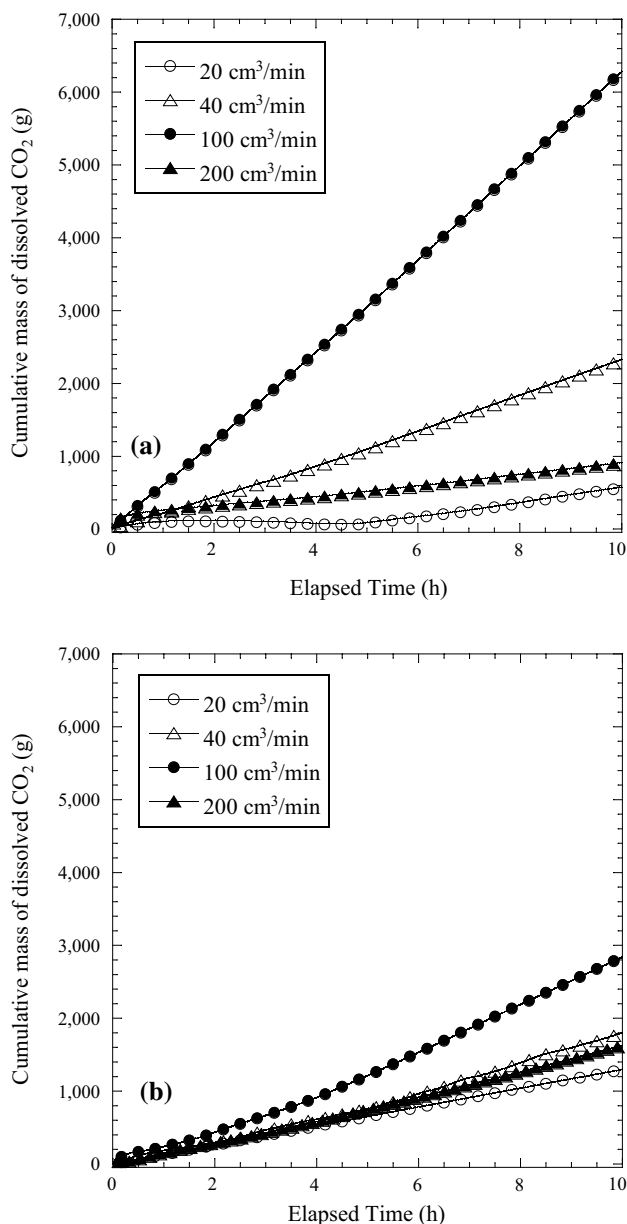


Fig. 9 Cumulative mass of dissolved CO₂ as a function of the elapsed time, obtained from the visualization experiments using finer (0.25–0.5 mm) and coarser (0.5–1.0 mm) glass beads at various CO₂ injection rates

lateral extent of the plume (i.e., CO₂ gas bubbles and dissolved CO₂) increases due to advection and diffusion, with the increase in the porous medium size and CO₂ exsolution rate. For the finer porous medium at a high CO₂ exsolution rate, CO₂ gas bubbles can coalesce to form gas clusters, while continuous channelized flow, without cluster formation, occurs in the coarser porous medium, regardless of the CO₂ exsolution rate (Fig. 3).

Once the plume (i.e., CO₂ gas bubbles and dissolved CO₂) reaches the interface between the saturated porous

medium and air or the unsaturated porous medium, the plume extends laterally on the surface, producing a thin, dense CO₂-saturated layer. Simultaneously, CO₂ gas is emitted from the saturated porous medium, leading to an increase in CO₂ gas concentration in the atmosphere. The grain size of the porous medium present in the shallow aquifer and the CO₂ exsolution rate affects the degree and pattern of the CO₂ gas emission. For example, for the coarser porous medium at a higher CO₂ exsolution rate, earlier and greater CO₂ gas emission can occur. In addition, continuous and periodic CO₂ gas emission can occur, depending on the grain size of the porous medium and the CO₂ exsolution rate (Figs. 7 and 8).

Conclusions

Visualization experiments using a rectangular transparent acrylic cell, which contained glass beads saturated with an alkaline solution having a universal pH indicator, were conducted to investigate the migration behavior of CO₂ gas and dissolved CO₂ in water-saturated porous media. The experiments indicated that the injected CO₂ leaked through the caprock, with the CO₂-saturated groundwater moving upward through the discontinuities, causing the exsolution of CO₂ gas from the CO₂-saturated groundwater. The CO₂ gas and the dissolved CO₂, after exsolution from the CO₂-saturated groundwater, can migrate through the porous media in shallow aquifers.

Immediately after the CO₂ gas injection ($t < 1$ s), which is comparable to the period immediately following the CO₂ exsolution, CO₂ gas moved upward due to buoyancy and pressure gradient, percolating into pores through various pathways. The CO₂ gas displaced the water in the pores of the glass beads, producing irregular continuous gas pathways, known as channelized flow. The continuous channelized flow was more dominant in coarser glass beads (0.75–1.0 mm), while transient channelized flow (i.e., gas clusters migration) occurred in the finer glass beads (0.25–0.50 mm).

During CO₂ gas injection ($t > 1$ s), CO₂ gas bubbles continued to move upward to the interface between the saturated porous medium and air, with the color of pore water near the pathways of CO₂ gas bubbles changing from blue (i.e., alkaline) to yellow (i.e., acidic), regardless of the grain size and the CO₂ gas injection rate, suggesting CO₂ dissolution in pore water near the CO₂ gas migration pathways. Once the CO₂ gas reached the interface, a thin, dense yellow layer (i.e., CO₂ dissolved water) was formed, laterally extending by advection and diffusion. After the formation of the thin, dense yellow layer, small fingers occurred, which subsequently gradually coalesced, thickening the dense yellow layer, indicating density-driven convection. The fingers due to density-driven convective flow occurred more clearly in the coarser glass beads. The migration of carbonated water was faster as both, the glass bead size and the CO₂ gas

injection rate, increased, causing earlier CO₂ saturation in pore water.

The temporal changes in the effluent CO₂ gas concentration emitted from the saturated glass beads to air varied with the grain size of the porous medium and the CO₂ gas injection rate. For the coarser glass beads, earlier and higher CO₂ gas emission generally occurred at a given CO₂ gas injection rate. As the CO₂ injection rate increased, the effluent CO₂ gas concentration was more stable.

The results of this study suggest that the extent and pattern of CO₂ gas emission from the ground surface can be implicitly predicted using information such as porous media properties and CO₂ exsolution rate and vice versa. However, the findings in this study are probably only applicable to specific conditions, without representing real field conditions, because the experiments in this study were conducted under specific and limited conditions, which might not represent real field conditions. Further study under various conditions (e.g., various grain sizes and CO₂ injection rates, heterogeneity of porous media) needs to be conducted to understand the patterns of CO₂ gas and dissolved CO₂ migration in porous media and CO₂ gas concentration in the boundary between the ground and atmosphere.

Acknowledgements This research was supported by the Korea Ministry of Environment (MOE) under the “K-COSEM Research Program” and the National Research Foundation (NRF-2017R1A2B4008238) of the Ministry of Science, ICT and Future Planning, Korea.

References

- Amonette JE, Barr JL, Erikson RL, Dobeck LM, Barr JL, Shaw JA (2013) Measurement of advective soil gas flux: results of field and laboratory experiments with CO₂. *Environ Ear Sci* 70(4):1717–1726
- ASTM D 422–63 (2007) Standard test method for particle-size analysis of soils. ASTM International, West Conshohocken, PA
- ASTM D 6836–16 (2016) Standard test method for determination of the soil water characteristic curve for desorption using hanging column, pressure extractor, chilled mirror hygrometer, or centrifuge. ASTM International, West Conshohocken, PA
- Bang ES, Son JS, Santamarina JC (2012) Subsurface CO₂ leakage: lab-scale study of salient characteristics and assessment of borehole-based detection using resistivity tomography. In: 4th International Conference on Geotechnical and Geophysical Site Characterization (ISC’4)
- Brooks MC, Wise WR, Annable MD (1999) Fundamental changes in in situ air sparging flow patterns. *Ground Water Monit Remediat* 19(2):105–113
- Cihan A, Corapcioglu MY (2008) The effect of compressibility on the rise velocity of an air bubble in porous media. *Water Resour Res* 44(W04409):1–8
- Corapcioglu MY, Cihan A, Drazenovic M (2004) Rise velocity of an air bubble in porous media: theoretical studies. *Water Resour Res* 40(W04214):1–9
- Dominguez A, Bories S, Prat M (2000) Gas cluster growth by solute diffusion in porous media. Experiments and automaton simulation on pore network. *Int J Multiph Flow* 26:1951–1979
- Enouy R, Li M, Ioannidis MA, Unger AJA (2011) Gas exsolution and flow supersaturated water injection in porous media: II. Column experiments and continuum modeling. *Adv Water Resour* 34:15–25
- Faisal TF, Chevalier S, Sassi M (2013) Experimental and numerical studies of density driven natural convection in saturated porous media with application to CO₂ geological storage. *Energy Proced* 37:5323–5330
- Foster LS, Grunfest IJ (1937) Demonstration experiments using universal indicators. *J Chem Educ* 14(6):274
- Gaus I (2010) Role and impact of CO₂-rock interactions during CO₂ storage in sedimentary rocks. *Int J Greenh Gas Con* 4:73–89
- Geistlinger H, Krauss G, Lazik D, Luckner L (2006) Direct gas injection into saturated glass beads: transition from incoherent to coherent gas flow pattern. *Water Resour Res* 42:W07403
- Holloway S (2005) Underground sequestration of carbon dioxide—a viable green-house gas mitigation option. *Energy* 30:2318–2333
- IEA/OECD (2008) CO₂ capture and storage—a key carbon abatement option. Organisation for Economic Co-operation and Development & International Energy Agency, Paris, p 266
- IPCC (2007) Climate change 2007: Synthesis report. In: Pachauri RK, Reisinger A (eds) IPCC, Geneva, p 104
- Ji W, Dahmani A, Ahlfeld DP, Lin JD, Hill IE (1993) Laboratory study of air sparging: air flow visualization. *Ground Water Monit Remediat* 13(4):115–116
- Kneafsey TJ, Pruess K (2009) Laboratory flow experiments for visualizing carbon dioxide-induced, density-driven brine convection. *Transp Porous Media* 82(1):123–139
- Kreft E, Bernstone C, Meyer R, May F, Arts R, Obdam A, Svensson R, Eriksson S, Durst P, Gaus I, Meer B, Geel C (2007) “The Schweinrich structure”, a potential site for industrial scale CO₂ storage and a test case for safety assessment in Germany. *Int J Greenh Gas Con* 1:69–74
- Li X, Yortsos YC (1995) Theory of multiple bubble growth in porous media by solute diffusion. *Chem Eng Sci* 50(8):1247–1271
- Mojtaba S, Behzad R, Rasoul NM, Mohammad R (2014) Experimental study of density-driven convection effects on CO₂ dissolution rate in formation water for geological storage. *J Nat Gas Sci Eng* 21:600–607
- Neufeld JA, Hesse MA, Riaz A, Hallworth MA, Tchelepi HA, Huppert HE (2010) Convective dissolution of carbon dioxide in saline aquifers. *Geophys Res Lett* 37:L22404
- Oldenburg CM, Lewicki JL (2006) On leakage and seepage of CO₂ from geologic storage sites into surface water. *Environ Geol* 50(5):691–705
- Plampin M, Illangasekare T, Sakaki T, Pawar R (2014) Experimental study of gas evolution in heterogeneous shallow subsurface formations during leakage of stored CO₂. *Int J Greenh Gas Control* 22:47–62
- Polak S, Cinar Y, Holt T, Torsæter O (2011) An experimental investigation of the balance between capillary, viscous, and gravitational forces during CO₂ injection into saline aquifers. *Energy Proced* 4:4395–4402
- Porter ML, Plampin M, Pawar R, Illangasekare T (2015) CO₂ leakage in shallow aquifers: a benchmark modeling study of CO₂ gas evolution in heterogeneous porous media. *Int J Greenh Gas Control* 39:51–61
- Roosevelt SE, Corapcioglu MY (1998) Air bubble migration in a granular porous medium: experimental studies. *Water Resour Res* 34(5):1131–1142
- Sakaki T, Plampin M, Rawar R, Komatsu M, Illangasekare T (2013) What controls carbon dioxide gas phase evolution in the subsurface? Experimental observations in a 4.5 m-long column under different heterogeneity conditions. *Int J Greenh Gas Control* 17:66–77
- Thomas C, Lemaigre L, Zalts A, D’Onofrio A, Wit AD (2015) Experimental study of CO₂ convective dissolution: the effect of color indicators. *Int J Greenh Gas Control* 42:525–533

Zhao K (2010) Experimental investigation of air injection in saturated unconsolidated porous media. University of Science and Technology of China, Guangdong

Zhou X, Apple ME, Dobeck LM, Cunningham AB, Spangler LH (2013) Observed response of soil O₂ concentration to leaked CO₂ from an engineered CO₂ leakage experiment. *Int J Greenh Gas Control* 16:116–128